Available online at www.sciencedirect.com
SCIENCE DIRECT®
Icarus 166 (2003) 229–237
ICARUS
www.elsevier.com/locate/icarus

Mapping of the cusp plasma precipitation on the surface of Mercury

S. Massetti,[a,*] S. Orsini,[a] A. Milillo,[a] A. Mura,[a] E. De Angelis,[a] H. Lammer,[b] and P. Wurz [c]

[a] *Istituto di Fisica dello Spazio Interplanetario, Consiglio Nazionale delle Ricerche, via Fosso del Cavaliere 100, I-00133 Roma, Italy*
[b] *Space Research Institute, Department of Extraterrestrial Physics, Austrian Academy of Sciences, Schmiedlstr. 6, A-8042 Graz, Austria*
[c] *Physikalisches Institut, University of Bern, Sidlerstr. 5, CH-3012 Bern, Switzerland*

Received 15 November 2002; revised 21 August 2003

Abstract

The presence of a magnetosphere around Mercury plays a fundamental role on the way the solar wind plasma interacts with the planet. Since the observations suggest that Mercury should occupy a large fraction of its magnetosphere and because of lack of an atmosphere, significant differences in solar wind-magnetosphere coupling are expected to exist with respect to the Earth case. On the basis of a modified Tsyganenko T96 model we describe the geometry of the magnetic field that could characterize Mercury, and its response to the variations of the impinging solar wind and of the interplanetary magnetic field. The investigation is focused on the shape and dimension of the open magnetic field regions (cusps) that allow the direct penetration of magnetosheath plasma through the exosphere of Mercury, down to its surface. The precipitating particle flux and energy are evaluated as a function of the open field line position, according to different solar wind conditions. A target of this study is the evaluation of the sputtered particles from the crust of the planet, and their contribution to the exospheric neutral particle populations. Such estimates are valuable in the frame of a neutral particle analyser to be proposed on board of the ESA/BepiColombo mission.

Keywords: Mercury; Magnetosphere; Solar wind; Magnetic field

1. Introduction

The presence of a magnetosphere around Mercury plays a fundamental role on the way the solar wind plasma interacts with the planet (e.g., Ness et al., 1976). On the other hand, the existence of a weak intrinsic magnetic field together with the absence of an atmosphere, leads to important differences between the magnetospheric phenomena acting on Earth and Mercury. The magnetosphere of Mercury has been the object of various studies (e.g., Goldstein et al., 1981; Slavin et al., 1997; Luhmann et al., 1998; Killen et al., 2001), and some of them discussed the interaction of the solar wind plasma with the planetary surface. Nevertheless, because of the small amount of data available (Mariner 10 flybys, see Ness et al., 1976), modelling the magnetic field of Mercury involves some uncertainty. The relevant amount of crucial physical issues related to Mercury's environment induced the international space agencies (NASA, ESA, and ISAS) to plan important space missions devoted to the exploration of this planet (Messenger and BepiColombo). The scientific community is now facing the challenge to design instruments and improve data processing according to the present knowledge and theoretical expectations.

The present work aims to realize a *tool of analysis* to be used for determining the different configurations that could occur on the basis of the variation of the input parameters within a range of realistic values, without pretending to depict an "exact" model of the magnetosphere of Mercury. The uncertainties arising from many factors (e.g.: the density of the exosphere, magnetic field strength and geometry, surface conductivity, and others) force us to focus on qualitative more than on quantitative aspects. On the basis of a modified Tsyganenko T96 model (Tsyganenko, 1996), we establish the geometry of the magnetic field that could characterize Mercury, and its response to the variations of the impinging solar wind. The investigation is focused on the shape and dimension of the regions characterized by open magnetic field (magnetospheric cusps) that allow the direct penetration of magnetosheath plasma through the exosphere of Mercury, down to its surface. Section 2 is focused on the solar wind condition at Mercury's orbit, the model of Mercury's mag-

* Corresponding author.
E-mail address: stefano.massetti@ifsi.rm.cnr.it (S. Massetti).

0019-1035/$ – see front matter
doi:10.1016/j.icarus.2003.08.005

netosphere and the magnetosheath properties. Section 3 describes the acceleration mechanism associated with the magnetic reconnection on the dayside magnetopause. Section 4 shows the characteristics of the open field related area on Mercury, and Section 5 illustrates the sputtering generated by the magnetosheath plasma interaction with Mercury's surface. Summary and discussion are given in Section 6.

2. Sun–Mercury relationship and input parameters

2.1. The solar wind at Mercury

The solar wind at Mercury's orbit (0.29–0.44 AU) differs substantially from the average condition present at 1 AU. The Parker's spiral forms an angle of about 20° with the solar wind direction, less than half of the value at the Earth's orbit ($\sim 45°$), which implies a change of the relative weight of the interplanetary magnetic field (IMF) components with respect to the near Earth conditions, thus modifying the solar wind—magnetosphere interaction. Burlaga (2001) reported the IMF at Mercury to be 3–6 times the average strength at 1 AU ($B(E) \sim 5$ nT); by assuming a mean value of 4.5 we have $B(M) = 4.5B(E) \sim 23$ nT, and by taking into account the direction of the Parker's spiral we can estimate the IMF tangential component at Mercury to be roughly $B_t(M) \sim \sin 20° B(M) \sim 8$ nT. In the case of Mercury, the contribution of the IMF B_y component is less relevant than at the Earth, so that the magnetic reconnection at the dayside magnetopause is essentially driven by the IMF B_z component. Moreover, the increasing weight of the IMF B_x component might play a role in the way the Mercury's magnetosphere links with the solar wind (e.g., Kabin et al., 2000; Sarantos et al., 2001). Nevertheless, we expect the IMF at the orbit of Mercury to be characterised by strong deviation from the nominal Parker spiral, especially during periods of high solar activity. In the present study we focused on the effects associated with the IMF tangential component and the B_x contribution is not taken into account. The average solar wind density is about a factor of ten higher than at the Earth's orbit, even if this value varies considerably due to the high eccentricity of the planetary orbit (Burlaga, 2001): in fact, using the formula derived from the data of *Helios* spacecraft between 0.3–1.0 AU (Bougeret et al., 1984):

$$N = 6.4 \times R^{-2.1}\ \mathrm{cm}^{-3} \quad (1)$$

we obtain $N_{\min} = 34\ \mathrm{cm}^{-3}$ at aphelion ($R = 0.44$ AU), $N_{\max} = 83\ \mathrm{cm}^{-3}$ at perihelion ($R = 0.29$ AU), and average value $N_{\mathrm{ave}} = 52\ \mathrm{cm}^{-3}$ ($R = 0.36$ AU), compared to $N \sim 6\ \mathrm{cm}^{-3}$ at 1 AU. Table 1 reports some important average values evaluated for $R = 0.36$ AU (e.g., Kabin et al., 2000; Burlaga, 2001).

Table 1
Average solar wind parameters at Mercury

Solar wind speed	$430\ \mathrm{km\,s}^{-1}$
Solar wind density	$52\ \mathrm{cm}^{-3}$
Solar wind ion temperature	$\sim 2 \times 10^5$ K
Dynamic pressure	16 nPa
Ion sound speed	$74\ \mathrm{km\,s}^{-1}$
Alfvén speed	$120\ \mathrm{km\,s}^{-1}$
Specific heat ratio (γ)	5/3
Mach number (M_∞)	5.8
Alfvénic Mach number ($M_{\mathrm{A}\infty}$)	3.6

2.2. Modeling the magnetosphere of Mercury

In the present work, we approximate the magnetosphere of Mercury by means of a modified Tsyganenko T96 model (Tsyganenko, 1996). This magnetospheric model version includes an explicitly defined realistic magnetopause, large-scale Region 1 and 2 Birkeland current systems, the IMF penetration across the magnetospheric boundary, and accepts both IMF B_y and B_z components as independent input parameters. We removed the contribution of the ring current, since Mercury's magnetic field seems to be not able to trap particles into closed drift paths around the planet, although the injection of plasma into the magnetosphere during magnetic substroms could generate at least a transient partial-ring current (e.g., Orsini et al., 2001; Lukyanov et al., 2001). Due to the expected lack of a conducting ionosphere on Mercury there is still a wide debate regarding the existence of field-aligned currents, together with the existence of mechanisms capable to allow the closure of the magnetospheric current systems. In the present work, our choice is to assume a 50% contribution of the Birkeland currents in the T96 model, that is an halfway position between the Earth's case and a null contribution. In addition, to address the differences of both the intensity of the magnetic field and the radius of Mercury with respect to the Earth, we have scaled the T96 model by a factor 6.9, like in previous analyses based on the *Mariner* 10 data (e.g., Luhmann et al., 1998). To find the open magnetic field lines (the field lines that cross the magnetopause and merge with the IMF), we used the subroutine *Locate* (Tsyganenko, 1996) that approximates the dayside magnetopause with an ellipsoid, as in the T96 model. In this context, it must be noted that, as well as other magnetospheric models, the T96 model does not describe the field depression caused by the diamagnetic effect of the plasma engulfing the magnetospheric cusps (Tsyganenko and Russell, 1999). To some extent, this lack causes a misrepresentation of the Mercury's magnetosphere/magnetopause on the dayside, which must be kept in mind when dealing with the cusp-related regions (low latitude boundary layer, cusp proper and mantle), since these areas are much wider on Mercury than on Earth.

2.3. The magnetosheath of Mercury

The magnetosheath is the region localized between the bow shock and the magnetopause (the thin current layer enveloping the magnetosphere), and it is populated by thermalised solar wind plasma that flows anti-sunward along the

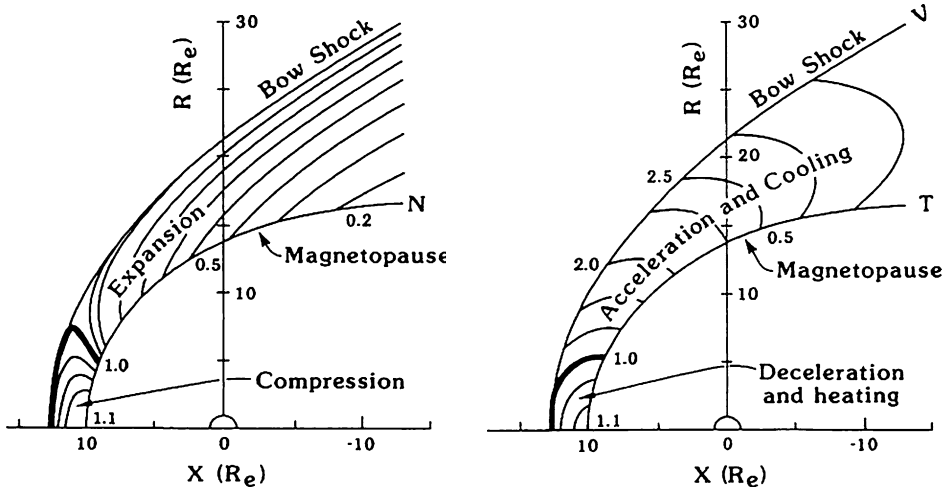

Fig. 1. Overall properties of the magnetosheath plasma parameters, density (N, left panel), velocity (V, right panel, upper values) and temperature (T, right panel, lower values), as a function of the position along the magnetosheath (after Song et al., 1999), and normalized to the unperturbed solar wind values.

flanks of the magnetosphere: the plasma is decelerated, compressed and heated in the subsolar region, then its speed increases progressively as the plasma moves tailward, with density and temperature gradually decreasing. In addition, on the dayside magnetosheath the frozen-in IMF dragged by the shocked solar wind plasma undergoes intensification, resulting from the compression of the plasma on the subsolar region. The parameters needed for defining the magnetosheath plasma environment were derived from the work of Spreiter et al. (1966), where the ratio of the local velocity (V), density (N), and temperature (T) with respect to the unperturbed upstream values (V_∞, N_∞, and T_∞), were calculated for an hydromagnetic flow around a magnetosphere (see Fig. 1).

In the Spreiter et al. (1966) work, most of the calculations were done for a gasdynamic free-stream Mach number ~ 8, which in the case of a magnetosphere should be more properly identified by a free-stream pseudo Mach number (Spreiter et al., 1966):

$$M^*_\infty = M_\infty M_{A_\infty} / \left(M^2_\infty + M^2_{A_\infty} - 1\right)^{1/2} \quad (2)$$

where M_∞ and M_{A_∞} are the free-stream Mach number and Alfvén Mach number, respectively, of the solar wind. We have extrapolated the V/V_∞, N/N_∞, and T/T_∞ variation along the magnetopause assuming that in the case of Mercury $M^*_\infty \sim 3$ (using data of Table 1), although the V/V_∞ ratio is roughly independent from M^*_∞. Then, these three parameters were fitted as a function of the distance from the subsolar point "d" along the GSM X-axis, as follow:

$$V/V_\infty = -0.249d + 0.953d^{1/2}, \quad (3)$$

$$N/N_\infty = 3.300 - 3.220d + 1.400d^{1.5}, \quad (4)$$

$$T/T_\infty = 1 + 3.000\left(1 - (V/V_\infty)^2\right). \quad (5)$$

Figure 2 shows V/V_∞ (solid line, right scale) and N/N_∞ (dashed line, left scale) in the upper panel, and T/T_∞ in the lower panel.

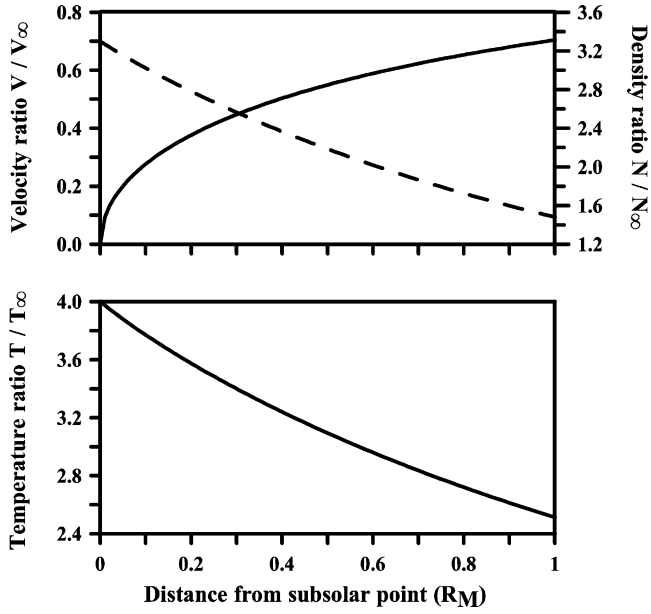

Fig. 2. Magnetosheath parameters variation along the magnetopause, as a function of the distance from the subsolar point, scaled to Mercury: T/T_∞ (lower panel), V/V_∞ (solid line, upper panel) and N/N_∞ (dashed line, upper panel).

3. A tool of analysis for the plasma precipitation at Mercury

3.1. Properties of the Earth's magnetospheric cusp regions

Before investigating the direct solar wind plasma entry into the magnetosphere of Mercury, we briefly describe in the following the configuration of the regions where this process takes place on the Earth's magnetosphere. Actually, the geomagnetic regions generally referred as *cusps* (one for each hemisphere) exhibit a complex structure. The cusp regions are usually divided into three sub-regions: the low latitude boundary layer (LLBL), the cusp proper (cusp)

and the mantle. The relative position and size of these sub-regions depend on the IMF B_y and B_z component, and when magnetic merging occurs at the dayside magnetopause with $B_z < 0$, the LLBL lies equatorward the cusp proper and the mantle poleward of it (e.g., Newell and Meng, 1992). The three regions are divided according to the energy and flux of the precipitating particles along those magnetic field lines that are connected to the IMF: the particle energy is at maximum in the LLBL and decreases when moving through the cusp and the mantle, while the particle flux has a maximum in the cusp proper.

The differentiation between the cusp sub-regions is also affected by a velocity filter effect, due to the fact that the higher the particle energy is (and speed), the less is the time it takes to flow along the field line: as a result, the lower energy particles are dragged at higher latitude as the open field line convects poleward. On the Earth, there is a step in the flux distribution between the LLBL and the cusp proper due to the existence of two distinct plasma populations in the magnetosheath: a lower energy component ($E < 1.3$ keV) with $\sim 80\%$ of the density, and a higher energy one ($E > 1.3$ keV) with the remaining 20% of the density (Fuselier et al., 1999). The hotter population is thought to be constituted by solar wind ions that, after being reflected back at the bow shock, perform a partial gyration into the upstream region before crossing the shock to enter the magnetopause (Fuselier et al., 1999, and references therein). This fact, associated with the velocity filter effect, causes the LLBL particles to be more energetic than expected on a basis of a single magnetosheath population.

3.2. Dayside magnetic reconnection and plasma entry

When the interplanetary magnetic field (which is compressed inside the magnetosheath) has a component that is antiparallel to the magnetospheric field near the magnetopause, a magnetic reconnection occurs between the two fields, and the magnetosheath plasma can cross the magnetopause and precipitate toward the planet. The reconnected fields generate a *rotational discontinuity* that moves away from the merging site, along the magnetopause itself. If the magnetopause is approximated as a one-dimensional discontinuity we can define a reference frame located on the discontinuity, called *de Hoffmann–Teller* frame (HT), where the reconnected field line is at rest. With respect to the planet, the HT frame moves along the magnetopause with velocity V_{HT}, which depends both on the flow velocity in the magnetosheath and on the magnetic tension due to the geometry of the reconnected field line. In the HT reference frame the energy and pitch angle are conserved, and the bulk flow on either side of the discontinuity is field-aligned and moving at the local Alfvén speed: in fact, by applying the tangential stress balance condition, one finds that the change in the momentum of the plasma must balance the magnetic field tension, and that the field-aligned speed of the plasma in the HT frame must be equal to the Alfvén speed in both the magnetosheath and the magnetosphere (Cowley and Owen, 1989; Cowley, 1995).

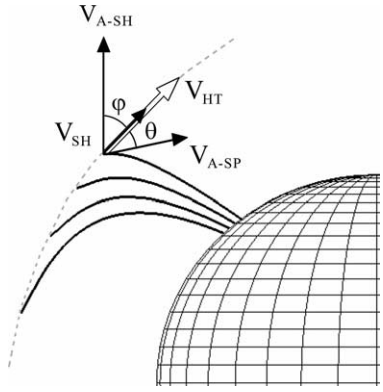

Fig. 3. Sketch of a reconnected field line on the dayside magnetopause, illustrating the parameters associated with the *de Hoffman–Teller* reference frame: $V_{\text{A-SH}}$ and $V_{\text{A-SP}}$ are the Alfvén speed on the magnetosheath and on the magnetosphere side, which are tangent to the local magnetic field; φ and θ are the angles formed by $V_{\text{A-SH}}$ and $V_{\text{A-SP}}$ with the magnetopause (dashed gray line); V_{SH} is the flow velocity in the magnetosheath (black arrow tangent to magnetopause); and V_{HT} is the HT reference frame velocity (white arrow).

Figure 3 depicts the geometry of a reconnected field line on the GSM XZ-plane (dayside, i.e., $X > 0$), assuming IMF pointing southward ($B_z < 0$): $V_{\text{A-SH}}$ and $V_{\text{A-SP}}$ are the Alfvén speed on the magnetosheath and on the magnetosphere side, which are tangent to the local magnetic field; φ and θ are the angles formed by $V_{\text{A-SH}}$ and $V_{\text{A-SP}}$ with the magnetopause (dashed gray line); V_{SH} is the flow velocity in the magnetosheath (black arrow tangent to magnetopause); and V_{HT} is the HT reference frame velocity (white arrow). In general, the aforementioned vectors do not lie on the same plane, and the stress balance condition in the HT frame can be written as (e.g.: Cowley and Owen, 1989; Lockwood and Smith, 1994; Cowley, 1995; Lockwood, 1995):

$$\overline{V}'_{\text{SH}} = \pm(V_{\text{A-SH}}\cos\varphi)\hat{b}_{\text{SH-MP}} \tag{6}$$

the upper (lower) sign refers to the Northern (Southern) hemisphere, where $V_{\text{A-SH}}$ is antiparallel (parallel) to the field line, and $\cos\varphi = \hat{b}_{\text{SH}} \cdot \hat{b}_{\text{SH-MP}}$, being $\hat{b}_{\text{SH}}$ and $\hat{b}_{\text{SH-MP}}$ the unit vector along the magnetosheath field line and its projection on the magnetopause, respectively. In the planet reference frame this translates to

$$\overline{V}_{\text{HT}} = \overline{V}_{\text{SH}} \mp (V_{\text{A-SH}}\cos\varphi)\hat{b}_{\text{SH-MP}}. \tag{7}$$

Since the minimum field-aligned velocity of the injected magnetosheath plasma is zero in the HT frame, in the planet frame we have:

$$\overline{V}_{\min} = (\overline{V}_{\text{HT}} \cdot \hat{b}_{\text{SP}})\hat{b}_{\text{SP}} \rightarrow V_{\min} = V_{\text{HT}}\cos\theta, \tag{8}$$

where $\hat{b}_{\text{SP}}$ is the unit vector along the magnetospheric field line. For the resulting peak and maximum field-aligned velocity of the magnetosheath distribution in the planet frame, we have:

$$\overline{V}_{\text{p}} = \overline{V}_{\min} + V_{\text{A-SP}}\hat{b}_{\text{SP}} \rightarrow V_{\text{p}} = V_{\text{HT}}\cos\theta + V_{\text{A-SP}}, \tag{9}$$

$$\overline{V}_{\max} = \overline{V}_{\rm p} + V_{\rm th}\hat{b}_{\rm SP} \rightarrow V_{\max} = V_{\rm HT}\cos\theta + V_{\text{A-SP}} + V_{\rm th}, \quad (10)$$

where $V_{\rm th}$ is the plasma thermal speed. From Eqs. (8)–(10) the corresponding energies $E_{\min}$, $E_{\rm p}$, and $E_{\max}$ can be calculated. In the present study the HT concept is applied to the dayside magnetopause of Mercury, assuming the magnetic field to be approximated by the modified T96 model described in Section 2.2.

4. LLBL, cusp, and Mantle precipitations on Mercury's surface

By applying of the above-described *tool of analysis*, we can outline the plasma entry through open field lines on the dayside surface of Mercury. In the following, the results of a preliminary analysis are shown, obtained by varying the input parameters within realistic ranges. We assume a 50% of the magnetosheath plasma on reconnected field lines to actually cross the magnetopause (the remaining 50% is reflected by the boundary) by applying a reflection factor of 0.5, which is a typical value in the case of the Earth (e.g., Lockwood, 1997). In addition, we estimated the fraction of the precipitating ions reaching the planet surface along reconnected field lines to be limited to particles with a pitch-angle smaller than 35° (loss cone angle), being the remaining ones reflected back due to the intensification of the magnetic field toward the planet. The pitch angle (α) limit is derived from the relation:

$$\sin^2\alpha = B_{\rm SS}/B_{\rm SURF}, \quad (11)$$

where the magnetic field strength at the subsolar point ($B_{\rm SS}$) and at the planet surface ($B_{\rm SURF}$) are about 100 and 300 nT, respectively. By combining the two aforementioned estimations we get an overall factor equal to 0.1, which means that only 10% of the nominal flux precipitates onto the planet.

To reduce the number of variables involved in the calculations, we consider the Alfvén speed in the magnetosheath to be constant and equal to $V_{\text{A-SH}} = 120$ km s^{-1} (Table 1), while the magnetospheric Alfvén speed is tentatively set to be $V_{\text{A-SP}} = 6V_{\text{A-SH}}$ (owing to the lower plasma density in the magnetosphere), because of the large uncertainties on the exospheric density distribution around Mercury (Lammer and Bauer, 1997; Lammer et al., 2003, *companion paper*; Wurz and Lammer, 2003). These values are in line with typical Alfvénic speeds at both outer and inner side of the Earth's magnetopause (e.g., Lockwood, 1997). The plasma thermal speed $V_{\rm th}$ affecting $V_{\max}$ (Eq. 10) and $E_{\max}$, is derived from the magnetosheath plasma temperature calculated by means of Eq. (5). For a 2×10^5 K solar wind, from Eq. (5) we get $T \sim 0.8 \times 10^6$ K at the subsolar point of the Mercury's magnetopause, to be compared with $T \sim 4.4 \times 10^6$ K in the case of the Earth, with a ratio of about 1/5. Finally, all the calculations were performed for the case of a zero tilt angle for the magnetic dipole of Mercury, which is a likely situation (Ness et al., 1976).

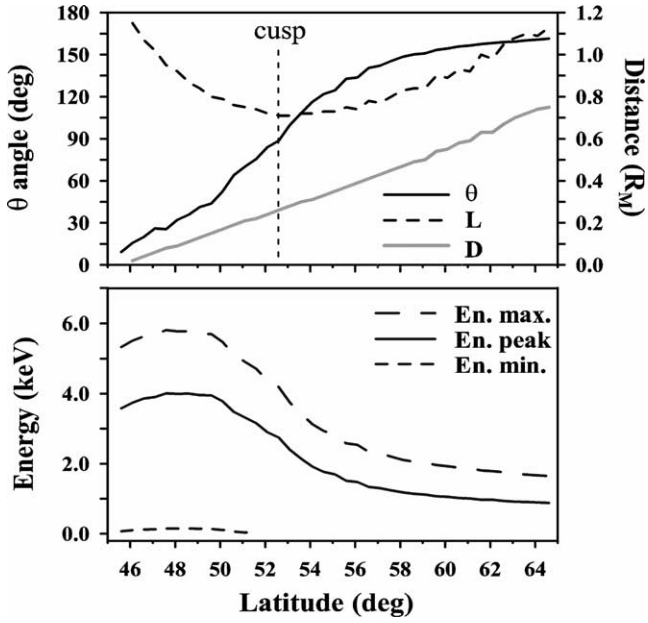

Fig. 4. Results obtained for an open field line moving on the XZ-plane (IMF $B_Z = -10$ nT). Upper panel: θ angle, open field line length (L) from planet surface to the magnetopause, and HT frame distance from the subsolar point (D) measured along the magnetopause. Lower panel: particle energy minimum, peak and maximum $E_{\min}$, $E_{\rm p}$, and $E_{\max}$. The vertical dotted line marks the nominal cusp location ($\theta = 90°$ and minimum of L).

Figure 4 shows typical parameters plotted as a function of latitude, characterizing the time evolution of a reconnected field line that moves from low to high latitudes along the meridian on the GSM XZ-plane (as depicted in Fig. 3), and calculated with a solar wind pressure $P_{\rm dyn} = 16$ nPa, IMF $B_y = 0$ nT, and IMF $B_z = -10$ nT. In the upper panel: θ angle, open field line length (L) from planet surface to the magnetopause, and distance (D) of the HT frame from the subsolar point measured along the magnetopause, the vertical dotted line marks the nominal cusp location, where $\theta = 90°$ and L is minimum. In the lower panel: particle distribution energies $E_{\min}$, $E_{\rm p}$, and $E_{\max}$. By comparing the two panels of Fig. 4, we can see that the injected particle energies: (a) initially increase as the field line straightens (LLBL, $\theta < 90°$, Lat $\sim 45°$–$49°$); (b) subsequently decrease to magnetosheath values in the cusp (no energy gain, $\theta \sim 90°$, Lat $\sim 53°$); (c) finally reach lower and lower values when the field line moves through the mantle ($\theta > 90°$, Lat $> 53°$). To minimize arbitrary hypotheses, in this preliminary study we neglected the *velocity filter effect*, and assumed the magnetosheath filled by just one plasma population (defined by the Eqs. (3)–(5)). In fact, part of the solar wind plasma impinging on the bow-shock of Mercury could be energised, giving rise to a second (hotter) magnetosheath plasma population, as happens at the Earth (Section 3.1). In this case, thanks to the *velocity filter effect*, the Mercury's LLBL will be more energetic than shown here, and there will be also a step in the energy between the LLBL itself and the cusp proper. However, the shape and size of the open field area, together with

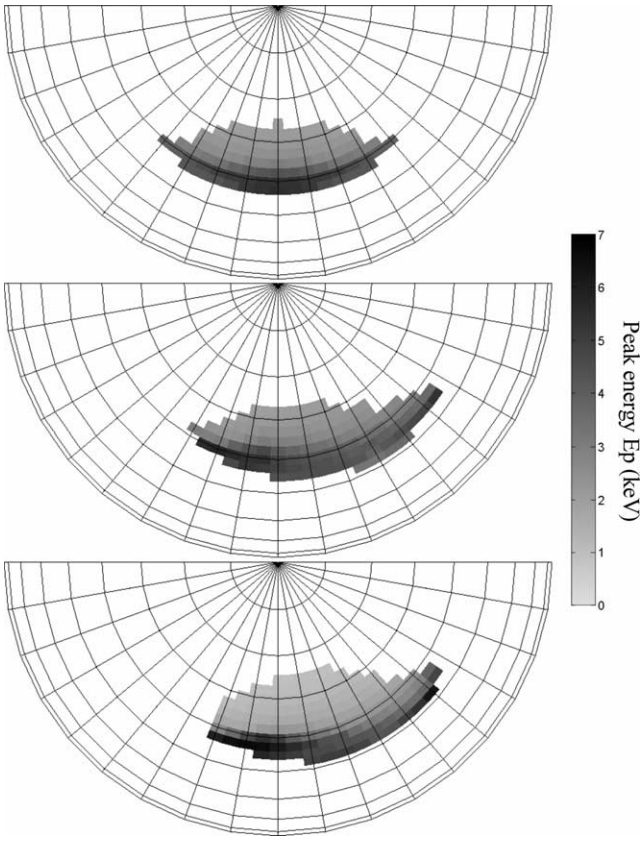

Fig. 5. Mapping of the open field area as a function of the incident peak energy (keV, left scale) on the northern dayside surface of Mercury (only the field lines crossing the magnetopause within $2R_M$ from the planet are considered). The three panels show the both area position and dimension according to different solar wind conditions: (top) $P_{dyn} = 16$ nPa, $B_y = 0$ nT, and $B_z = -10$ nT; (middle) $P_{dyn} = 16$ nPa, $B_y = -5$ nT, and $B_z = -10$ nT; (bottom) $P_{dyn} = 60$ nPa, $B_y = -5$ nT, and $B_z = -10$ nT.

the mean flux of the precipitating particles, are not affected by these choices, as most of the results derived here.

The three panels of Fig. 5 show both position and extension of the surface area with open field lines (AO), mapped on the northern dayside surface of Mercury in response to different solar wind conditions. The area is gray-coded according to the energy E_p of the particle distribution. We mapped only the open field lines that cross the magnetopause within $2R_M$ (the field lines at higher latitudes are open indeed, but the rate of solar wind plasma entry is low, since they map far in the magnetic tail), by using a 5° longitude per 2.5° latitude grid. The three configurations were calculated for: $P_{dyn} = 16$ nPa ($V_{sw} = 400$ km s^{-1}, $N_{sw} = 60$ cm^{-3}), $B_y = 0$ nT, and $B_z = -10$ nT (top panel), $P_{dyn} = 16$ nPa, $B_y = -5$ nT, and $B_z = -10$ nT (middle panel), $P_{dyn} = 60$ nPa ($V_{sw} = 600$ km s^{-1} and $N_{sw} = 100$ cm^{-3}), $B_y = -5$ nT, and $B_z = -10$ nT (bottom panel). By comparing Figs. 4 and 5, we notice that most of the energy (and flux) of the precipitating magnetosheath particles is deposited on a region that is narrow in latitude, but conversely extended in longitude. This region can be identified as low latitude boundary layer (LLBL, $\theta < 90°$), while the remaining area is characterized by a monotonous decrease of both energy and flux of the precipitating particles. In the upper panel of Fig. 5 we can observe what should be a typical configuration of the open field area of Mercury's cusps during moderate southward pointing IMF, under the assumption of a typical solar wind pressure at 0.36 AU (16 nPa): the open area ranges between about 45° and 65° in latitude, and about −40° and 40° in longitude. In the middle panel we see the effect associated with a negative IMF B_y (causing the shift of cusp proper toward dawn) that drags the whole open area eastward. In this case, the open area expands equatorward to about 40° latitude, and the most intense precipitation occurs on the South–West edge of the open area itself. Finally, the effect associated by a strengthening of the solar wind pressure up to 60 nPa is shown in the lower panel of Fig. 5. The open area shifts slightly eastward and expands poleward, mostly on the North–East edge. The ramming of the solar wind over the Mercury's magnetosphere causes a strong tailward bending of the magnetic field lines, and inhibits the particle precipitation at high latitudes, focusing the plasma entry on the equatorial edge of the open area. This effect is associated with an increase of both particle flux and energy, due to the rise of V_{sw} and/or D_{sw} that causes the P_{dyn} intensification. It must be stressed that all the above considerations apply also to the southern magnetic cusp, apart the fact that the IMF B_y effect reverses in this hemisphere.

When comparing the results of Fig. 5 with those of Sarantos et al. (2001) (Figs. 2 and 4), derived on the basis of the TH93 magnetospheric model (Toffoletto and Hill, 1993) with the explicit contribution of the IMF B_x component, we note a substantial match of the longitudinal extent of the open field area (about 80°–90°) and its displacement in response of IMF B_y variations. Nevertheless, a difference exists about the open area latitudinal width: their interval ranges between 60° to 10°–20° (IMF $B_z = -5$ nT and −20 nT, respectively) in latitude, to be compared with our range of about 65°–45°. In the TH93 model, the main effects of a strong IMF B_x are a North–South asymmetry and an equatorward expansion of the cusp region. The Sarantos et al. (2001) analysis was performed with a rather low solar wind pressure $P_{dyn} = 3.4$ nPa (four times smaller than the mean values at Mercury), and by assuming the penetration fraction of the IMF through the magnetopause (which is a free parameter of the TH93 model) to be as high as 40%, twice the Earth's case. Since both values affect the geometry of the magnetic field lines, the above comparison should be considered as only indicative.

The size of the open field associated area is an important parameter for characterizing the plasma precipitation on the planet, and we derived the dependence of the area size with respect to the IMF B_z (Fig. 6, upper panel) and to the solar wind pressure P_{dyn} (Fig. 6, lower panel). In the upper panel the open area is calculated with constant $P_{dyn} = 20$ nPa ($V_{sw} = 450$ km s^{-1}, $N_{sw} = 60$ cm^{-3}), while in the lower one with a constant IMF $B_z = -10$ nT, and by assuming IMF $B_y = 0$ nT in both cases. We see that the open field area is

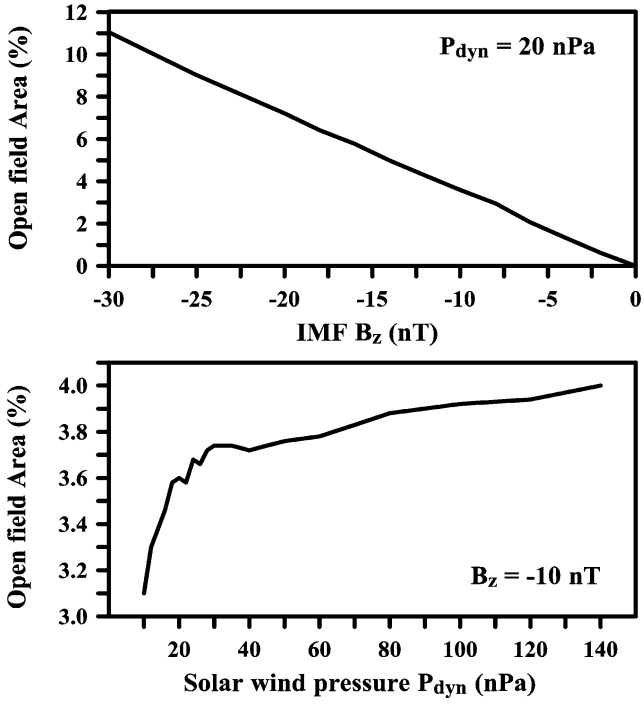

Fig. 6. Open field area (AO) of Mercury's cusps as a function of the IMF B_z component (upper panel), and of the solar wind pressure $P_{\rm dyn}$ (lower panel). The two sets of data were derived with IMF $B_y = 0$, together with the IMF B_z and $P_{\rm dyn}$ values indicated in the legends.

Table 2
Mean values of particle flux and open field area at Mercury ($P_{\rm dyn} = 20$ nPa)

IMF B_z (nT)	Open field area (cm^2)	Particle flux (cm^{-2} s^{-1})	Open field area rate (s^{-1})
−10	2.8×10^{16}	4.1×10^{8}	1.1×10^{25}
−20	5.4×10^{16}	3.8×10^{8}	2.1×10^{25}
−30	8.3×10^{16}	3.7×10^{8}	3.0×10^{25}

more modulated by IMF B_z than by $P_{\rm dyn}$ variations. The dependence on IMF B_z is nearly linear and can be expressed as:

$$\mathrm{AO}(\%) \sim -0.36 B_z \ (\mathrm{nT}). \tag{12}$$

The dependence on $P_{\rm dyn}$ is weak and exhibits a kink at about 30 nPa (in the present case where IMF $B_z = -10$ nT); two linear relations can tentatively approximate the trend:

$$\mathrm{AO}(\%) \sim 2.962 + 0.028 P_{\rm dyn} \ (\mathrm{nPa}), \quad P_{\rm dyn} < 30 \ \mathrm{nPa}, \tag{13a}$$

$$\mathrm{AO}(\%) \sim 3.624 + 0.003 P_{\rm dyn} \ (\mathrm{nPa}), \quad P_{\rm dyn} > 40 \ \mathrm{nPa}. \tag{13b}$$

In a first approximation, and within the assumptions considered, the effect of the solar wind pressure on the open field related area can be assumed to be negligible. As reference, Table 2 shows three mean values of the open field area and particle flux at Mercury, computed for IMF $B_z = -10$, -20, -30 nT, and $P_{\rm dyn} = 20$ nPa. The mean particle flux through the open field area (last column) increases by a factor proportional to |IMF $B_z/10$ nT|, while the mean particle flux itself decreases slightly due to the increase of the relative weight of the low flux regions (cusp proper and mantle). As a realistic upper limit for the particle flux precipitation we get the value of about 2×10^9 cm^{-2} s^{-1}, obtained with $P_{\rm dyn} =$ 164 nPa ($V_{\rm sw} = 700$ km s^{-1}, $N_{\rm sw} = 200$ cm^{-3}), $V_{\text{A-SH}} =$ 180 km s^{-1}, and $V_{\text{A-SP}}/V_{\text{A-SH}} = 8$, which leads to a mean particle flux across the Mercury's cusps of $\sim 10^{26}$ s^{-1}.

5. Discussion: surface sputtering and ENA production from cusp-mapped surface of Mercury

Where the open field lines intersect the planetary surface, the soil becomes directly linked to the magnetosheath plasma population, and then exposed to ion precipitation. The ion impact on the soil leads to a particle release process called "ion-sputtering" (e.g., Lammer and Bauer, 1997; Killen et al., 2001; Lammer et al., 2003; Wurz and Lammer, 2003). The sputtered particles follow ballistic trajectories, before falling back to the surface or escaping from the planet, depending on their initial energy and direction. The energy distribution for sputtered particles, $F(E_{\rm e})$, with ejection energy $E_{\rm e}$, can be expressed as (Sieveka and Johnson, 1984):

$$F(E_{\rm e}) \sim \frac{E_{\rm e}}{(E_{\rm e} + E_{\rm b})^3} \left[1 - \sqrt{\frac{E_{\rm e} + E_{\rm b}}{E_{\rm i}}} \right], \tag{14}$$

where $E_{\rm i}$ is the energy of the incident particle and $E_{\rm b}$ is the surface binding energy of the sputtered particle. The products arising from this particle bombardment depend both on the composition and chemical structure of the planet surface. In the case of Mercury, the small amount of data does not allow any precise estimate of the surface composition. However, the presence of H, He, O, Na, K, and Ca in the exosphere of the planet was established by both space and ground-based observations (Broadfoot et al., 1976; Potter and Morgan, 1986; Bida et al., 2000). Because the sodium spatial and temporal distribution was found to be compatible with solar activity variations (Killen et al., 2001), sputtering may be an important process. Since sodium is likely bound to oxygen (oxide composites), the binding energy could be assumed to be 2 eV (McGrath et al., 1986). Figure 7 shows the normalized integral of $F(E_{\rm e})$, from $E_{\rm e}$ to infinity, as a function of ejected particle energy $E_{\rm e}$, in the case of $E_{\rm i} = 1$ keV solar wind protons (assuming an overall binding energy for oxygen equal to 4 eV, Lammer and Bauer, 1997).

If we derive $F(E_{\rm e})$ from Eq. (14) and then apply the estimated precipitating ion fluxes as obtained in the analysis performed in the previous paragraph, we can estimate the neutral atom (ENA) fluxes extracted by the soil of Mercury. Figure 8 shows an estimation of the sputtered Na-ENA (right scale) and O-ENA (left scale) fluxes, induced by the magnetosheath plasma precipitating throughout the Mercury's northern cusp. The fluxes are calculated by using the surface sputter yield derived in our companion paper (Lammer

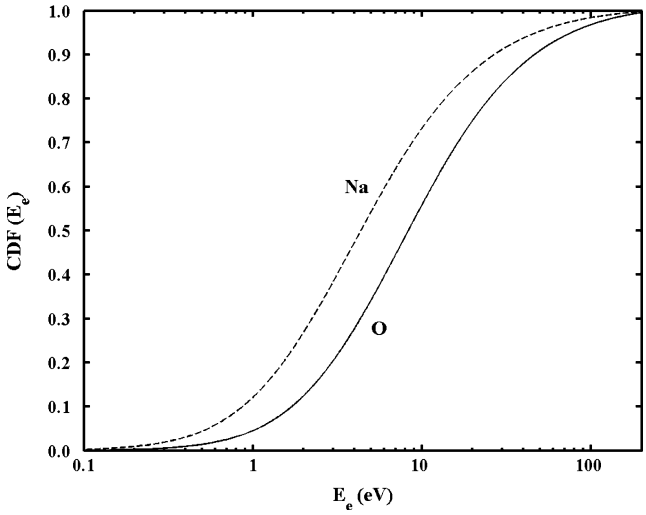

Fig. 7. Normalized integral (from E_e to infinity) of the energy distribution of Na and O sputtered particles, as a function of their ejection energy E_e, in the case of $E_i = 1$ keV solar wind protons.

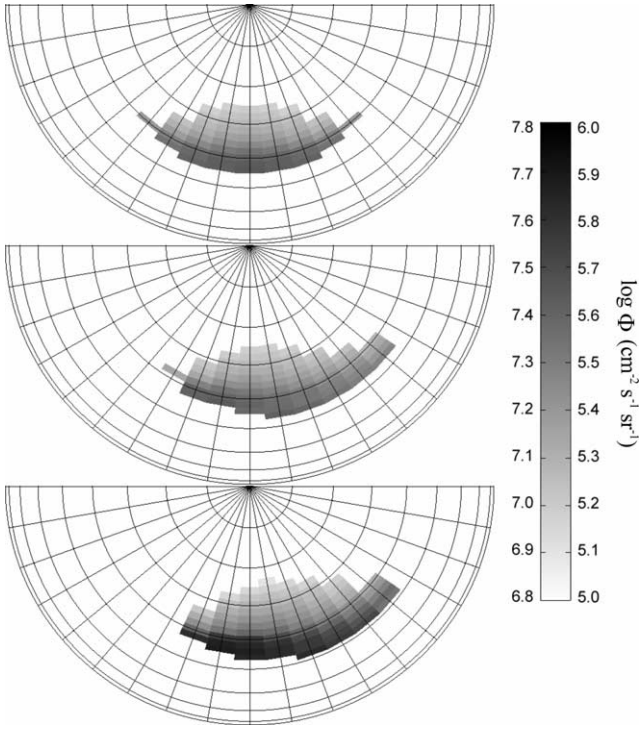

Fig. 8. Gray-coded Na-ENA (right scale) and O-ENA (left scale) flux spatial distribution (calculated assuming an energy E_p for all precipitating particles) generated by ion-sputtering from the open field area, on the northern dayside surface of Mercury. As in Fig. 5, the three panels refer to different solar wind conditions: (top) $P_{dyn} = 16$ nPa, $B_y = 0$ nT, and $B_z = -10$ nT; (middle) $P_{dyn} = 16$ nPa, $B_y = -5$ nT, and $B_z = -10$ nT; (bottom) $P_{dyn} = 60$ nPa, $B_y = -5$ nT, and $B_z = -10$ nT.

et al., 2003), 0.07 for sodium and 0.03 for oxygen in the case of 1 keV proton impacts, and by assuming a relative abundance of 0.0053 for sodium and 0.8 for oxygen in the soil of Mercury. Moreover, we consider that all precipitating ions have the same energy E_p (corresponding to the magnetosheath distribution peak as derived from Eq. (9)), and that the energy distribution of the sputtered particles is integrated above the energy corresponding to the escape velocity from the planet (4.3 km s^{-1} $\sim$ 2 eV for Na).

Using the same input values of Fig. 5 we derived the three patterns illustrated in Fig. 8. According to the patterns depicted in Fig. 5, the ENA induced by ion-sputtering have a distribution peaked in a narrow band on the equatorward edge of the open field area (upper panel). The ENA distribution is stretched in longitude, with a East–West displacement controlled by the IMF B_y (middle panel). An increasing solar wind pressure P_{dyn} (due to an increase of V_{sw} and/or N_{sw}) causes the widening of the sputtered area and an intensification of the signal (lower panel). Within the ion-sputtering context, the solar wind plasma precipitating through cusp regions can be seen as a beam that probes the planet surface, and induces a signal whose geographical extension and intensity depend on the incoming solar wind conditions, whereas its mass spectrum is strongly related to the atomic composition of the soil.

6. Summary

We modelled the solar wind interaction with the magnetosphere of the planet Mercury by means of a numerical *tool of analysis*. Our study is focused on the direct solar wind plasma entry through the magnetic cusps of Mercury. In particular, details on the size and shape of the regions where the open magnetic field lines map, as well as on the particles acceleration generated by the magnetic reconnection with the interplanetary magnetic field are given. For IMF $B_z = -10$ nT, we found a mean open field area of 2.8×10^{16} cm^2, a mean proton flux of 4.1×10^8 cm^{-2} s^{-1}, and a proton precipitation rate via open field area of 1.1×10^{25} s^{-1}. We evaluated also the upper limit of the mean proton flux precipitating along open field lines, under *non-extreme* solar wind conditions, to be of the order of 2×10^9 cm^{-2} s^{-1}. For the first time, a pattern of the plasma precipitation through the open dayside magnetosphere of Mercury as a function of the particle energy is given. The acceleration produced by the magnetic reconnection on the dayside magnetopause seems to be able to increase the solar wind plasma energy up to several keV, while the reconnection mechanism itself causes the most energized particles to fall within a narrow band on the equatorward edge of the open field area, while the rest of the open field area is populated by particles with monotonously decreasing energy. In addition, we simulated the ENA signal produced by Na sputtered atoms, under different solar wind conditions, according to the sputtering yield calculated in our companion paper (Lammer et al., 2003). The ENA signal derived reveals to be a proxy of the solar wind plasma precipitation pattern through the open field lines.

The determination of the energy and flux precipitation pattern is useful for the analysis of the phenomena related to the direct solar wind plasma interaction with the surface

of Mercury, as particle release by ion-sputtering, resulting in thermal and non-thermal atom emission. The ENA signal is triggered by the state of the impinging solar wind, and its mass spectrum is expected to reflect the surface atomic composition, possibly giving information on the elemental composition of the Mercury surface.

A Neutral Particle Analyser (NPA-SERENA) is proposed for the ESA BepiColombo mission to Mercury. This detector consists of three spectrometers, capable to detect neutral atoms from thermal energies up to tens of keV, with high time and space resolution. NPA-SERENA will be able to monitor the sputtering-induced refilling of the exosphere, as well as the high-energy part of the non-thermal (directional) neutrals. Such measurements will allow the investigation of the solar wind interaction with the surface, providing new insights on the exosphere together with surface composition and erosion processes.

Acknowledgments

Authors thank N. Tsyganenko and the NASA/Goddard Space Flight Center for making magnetospheric models available to the scientific community. Referees are acknowledged for useful comments.

References

Bida, T.A., Killen, R.M., Morgan, T.H., 2000. Discovery of calcium in Mercury's atmosphere. Nature 404, 159–161.

Broadfoot, A.L., Shemansky, D.E., Kumar, S., 1976. Mariner 10: Mercury atmosphere. Geophys. Res. Lett. 3, 557–580.

Bougeret, J.L., King, J.H., Schwenn, R., 1984. Solar radio burst and in situ determination of interplanetary electron density. Solar Phys. 90, 401–412.

Burlaga, L.F., 2001. Magnetic fields and plasma in the inner heliosphere: helios results. Planet. Space Sci. 49, 1619–1627.

Cowley, S.W.H., 1995. Theoretical perspectives of the magnetopause: a tutorial review. In: Physics of the Magnetopause. In: AGU Geophysical Monograph, Vol. 90, pp. 29–43.

Cowley, S.W.H., Owen, C.J., 1989. A simple illustrative model of open flux tube motion over the dayside magnetopause. Planet. Space Sci. 37, 1461–1475.

Fuselier, S.A., Lookwood, M., Onsager, T.G., Peterson, W.K., 1999. The source population for the cusp and cleft/LLBL for southward IMF. Geophys. Res. Lett. 26, 1665–1668.

Goldstein, B.E., Suess, S.T., Walker, R.J., 1981. Mercury: magnetospheric processes and the atmospheric supply and loss rates. J. Geophys. Res. 86, 5485–5499.

Kabin, K., Gombosi, T.I., DeZeeuw, D.L., Powell, K.G., 2000. Interaction of Mercury with the solar wind. Icarus 143, 397–406.

Killen, R.M., Potter, A.E., Reiff, P., Sarantos, M., Jackson, B.V., Hick, P., Giles, B., 2001. Evidence for space weather at Mercury. J. Geophys. Res. 106, 20509–20525.

Lammer, H., Bauer, S.J., 1997. Mercury's exosphere: origin of surface sputtering and implications. Planet. Space Sci. 45, 73–79.

Lammer, H., Wurz, P., Patel, M.R., Killen, R., Kolb, C., Massetti, S., Orsini, S., Milillo, A., 2003. The variability of Mercury's exosphere by particle and radiation induced surface release processes. Icarus 166, 238–247.

Lockwood, M., 1995. Location and characteristics of the reconnection X line deduced from low-altitude satellite and ground-based observations. 1. Theory. J. Geophys. Res. 100, 21791–21802.

Lockwood, M., 1997. Energy and pitch-angle dispersion of LLBL/cusp ions seen at middle altitudes: prediction by the open magnetosphere model. Ann. Geophys. 15, 1501–1514.

Lockwood, M., Smith, M.F., 1994. Low and middle altitude cusp particle signatures for general magnetopause reconnections. 1. Theory. J. Geophys. Res. 99, 8531–8553.

Luhmann, J.G., Russell, C.T., Tsyganenko, N.A., 1998. Disturbances in Mercury's magnetosphere: are the Mariner 10 "substorms" simply driven? J. Geophys. Res. 103, 9113–9119.

Lukyanov, A.V., Barabash, S., Lundin, R., Brandt Jr., P.C., 2001. Energetic neutral atom imaging of Mercury's magnetosphere. 2. Distribution of energetic charged particles in a compact magnetosphere. Planet. Space Sci. 49, 1677–1684.

McGrath, M.A., Johnson, R.E., Lanzerotti, L.J., 1986. Sputtering of sodium on the planet Mercury. Nature 323, 694–696.

Ness, N.F., Behannon, K.W., Lepping, R.P., Whang, Y.C., 1976. Observations of Mercury's magnetic field. Icarus 28, 479–488.

Newell, P.T., Meng, C.-I., 1992. Mapping the dayside ionosphere to the magnetosphere according to particle precipitation characteristics. Geophys. Res. Lett. 19, 609–612.

Orsini, S., Milillo, A., De Angelis, E., Di Lellis, A.M., Zanza, V., Livi, S., 2001. Remote sensing of Mercury's magnetospheric plasma environment via energetic neutral atoms imaging. Planet. Space Sci. 49, 1659–1668.

Potter, A.E., Morgan, T.H., 1986. Potassium in the atmosphere of Mercury. Icarus 67, 336–340.

Sarantos, M., Reiff, P.H., Hill, T.H., Killen, R.M., Urquhart, A.L., 2001. A B_x-interconnected magnetosphere model for Mercury. Planet. Space Sci. 49, 1629–1635.

Sieveka, E.M., Johnson, R.E., 1984. Ejection of atoms and molecules from Io by plasma-ion impact. Astrophys. J. 287, 418–426.

Slavin, J.A., Owen, J.C.J., Connerney, J.E.P., Christon, S.P., 1997. Mariner 10 observations of field-aligned currents at Mercury. Planet. Space Sci. 45, 133–141.

Song, P., Russell, C.T., Gombosi, T.I., Spreiter, J.R., Stahara, S.S., Zhang, X.X., 1999. On the processes in the terrestrial magnetosheath. 1. Scheme development. J. Geophys. Res. 104, 22345–22355.

Spreiter, J.R., Summers, A.L., Alksne, A.Y., 1966. Hydromagnetic flow around the magnetosphere. Planet. Space Sci. 14, 223–253.

Toffoletto, F.R., Hill, T.W., 1993. A nonsingular model of the open magnetosphere. J. Geophys. Res. 98, 1339–1344.

Tsyganenko, N.A., 1996. Effects of the solar wind conditions on the global magnetospheric configuration as deduced from data-based field models. In: Proc. of 3rd International Conference on Substorms (ICS-3). In: ESA SP, Vol. 389, pp. 181–185.

Tsyganenko, N.A., Russell, C.T., 1999. Magnetic signatures of the distant polar cusp: observations by polar and quantitative modelling. J. Geophys. Res. 104, 24939–24956.

Wurz, P., Lammer, H., 2003. Monte Carlo simulation of Mercury's exosphere. Icarus 164, 1–13.